Photoinduced Electron Transfer in the Cytochrome c /Cytochrome c Oxidase Complex Using Thiouredopyrenetrisulfonate−Labeled Cytochrome c . Optical Multichannel Detection †

ARTICLE *in* BIOCHEMISTRY · MARCH 2001

Impact Factor: 3.02 · DOI: 10.1021/bi002341v · Source: PubMed

5 AUTHORS, INCLUDING:

Jenny Cappuccio
Humboldt State University
18 PUBLICATIONS **353** CITATIONS
SEE PROFILE

Natalia Borovok
Tel Aviv University
33 PUBLICATIONS **530** CITATIONS
SEE PROFILE

Photoinduced Electron Transfer in the Cytochrome *c*/Cytochrome *c* Oxidase Complex Using Thiouredopyrenetrisulfonate-Labeled Cytochrome *c*. Optical Multichannel Detection†

Istvan Szundi,‡ Jenny A. Cappuccio,‡ Natalia Borovok,§ Alexander B. Kotlyar,§ and Ólöf Einarsdóttir*,‡

Department of Chemistry and Biochemistry, University of California at Santa Cruz, Santa Cruz, California 95064, and Department of Biochemistry, George S. Wise Faculty of Life Sciences, Tel Aviv University, Ramat Aviv 69978, Israel

Received October 6, 2000

ABSTRACT: Intramolecular electron transfer in the electrostatic cytochrome *c* oxidase/cytochrome *c* complex was investigated using a novel photoactivatable dye. Laser photolysis of thiouredopyrenetrisulfonate (TUPS), covalently linked to cysteine 102 on yeast iso-1-cytochrome *c*, generates a triplet state of the dye, which donates an electron to cytochrome *c*, followed by electron transfer to cytochrome *c* oxidase. Time-resolved optical absorption difference spectra were collected at delay times from 100 ns to 200 ms between 325 and 650 nm. On the basis of singular value decomposition (SVD) and multiexponential fitting, three apparent lifetimes were resolved. A sequential kinetic mechanism is proposed from which the microscopic rate constants and spectra of the intermediates were determined. The triplet state of TUPS donates an electron to cytochrome *c* with a forward rate constant of $\sim 2.0 \times 10^4$ s^{-1}. A significant fraction of the triplet returns back to the ground state on a similar time scale. The reduction of cytochrome *c* is followed by faster electron transfer from cytochrome *c* to Cu_A, with the equilibrium favoring the reduced cytochrome *c*. Subsequently, Cu_A equilibrates with heme *a* with an apparent rate constant of $\sim 1 \times 10^4$ s^{-1}. On a millisecond time scale, the oxidized TUPS returns to the ground state and heme *a* becomes reoxidized. The extracted intermediate spectra are in excellent agreement with model spectra of the postulated intermediates, supporting the proposed mechanism.

Electron transfer from cytochrome *c* to the dioxygen site in cytochrome *c* oxidase has been extensively investigated using stopped-flow techniques (*1*). However, these measurements are limited by the rate of cytochrome *c* binding to cytochrome *c* oxidase (*2*, *3*). To circumvent this rate limitation, transient kinetic measurements using pulse radiolysis (*4*, *5*) or photoactivatable compounds as electron donors (*6*−*10*) have been carried out. While many of the early stopped-flow measurements pointed toward heme *a* and not Cu_A[1] being the initial electron acceptor from cytochrome *c*, the transient kinetic measurements suggested the opposite. For instance, the reduction of cytochrome *c* oxidase by the 1-methylnicotinamide (MNA) radical generated by pulse radiolysis indicated that Cu_A was the initial acceptor of electrons from cytochrome *c* (*4*). The apparent rate constant for electron transfer from Cu_A to heme *a* was found to be 1.8×10^4 s^{-1}. The same value was obtained during photoinduced electron transfer from tris(2,2′-bipyridyl)-ruthenium(II) bound to cytochrome *c* oxidase through electrostatic interactions (*6*) and following photodissociation of the three-electron-reduced CO-bound cytochrome *c* oxidase (*11*). Single-turnover flow-flash studies of the reaction of dioxygen with the electrostatic cytochrome *c*/cytochrome *c* oxidase complex provided further support for Cu_A being the initial acceptor of electrons from cytochrome *c* (*12*). The postulated rate constant for electron transfer between cytochrome *c* and Cu_A was greater than 7×10^4 s^{-1}. A similar value (6×10^4 s^{-1}) was recently obtained using laser-induced electron injection from Ru-modified cytochrome *c* (*9*).

Recent studies have used photoexcitation of thiouredopyrenetrisulfonate (TUPS), covalently linked to lysine residues on cytochrome *c*, to initiate electron transfer (*13*, *14*). In the work reported here, we used photoexcitation of TUPS covalently attached to cysteine 102 of yeast iso-1-cytochrome *c* to investigate electron transfer in the electrostatic cytochrome *c*/cytochrome *c* oxidase complex. The intramolecular electron transfer was monitored using multichannel detection. On the basis of singular value decomposition (SVD) and global exponential fitting of the time-resolved absorption difference spectra, a sequential kinetic mechanism for intramolecular electron transfer is proposed from which the microscopic rate constants and spectra of the intermediates are determined.

† This work was supported by the Israel-United States Binational Science Foundation (Grant 538/95) and by National Institutes of Health Grant GM 53788 (Ó.E.).

* To whom correspondence should be addressed. E-mail: olof@chemistry.ucsc.edu. Fax: (831) 459-2935.

‡ University of California.

§ Tel Aviv University.

[1] Abbreviations: TUPS, thiouredopyrene-3,6,8-trisulfonate; TUPS*, excited triplet state of TUPS; SVD, singular-value decomposition; *b*-spectrum, spectral changes associated with a particular first-order process; τ, apparent lifetime (1/rate constant); Cu_A, mixed-valence copper A center; Cu_B, copper B; a^{2+}, reduced heme *a*; a^{3+}, oxidized heme *a*; a_3^{2+}, reduced heme a_3; a_3^{3+}, oxidized heme a_3.

10.1021/bi002341v CCC: $20.00
Published on Web 01/25/2001

MATERIALS AND METHODS

Cytochrome *c* oxidase was isolated from bovine hearts according to the method of Yoshikawa et al. (*15*). The final precipitate was dissolved in 0.1 M sodium phosphate buffer (pH 7.4) and dialyzed overnight against the same buffer. The TUPS-cystamine and TUPS(Cys102)−iso-1-cytochrome *c* derivative were prepared as described previously (*16*). Briefly, the 1-isothiocyanatopyrene-3,6,8-trisulfonate was incubated with cystamine to form TUPS-cystamine. Following separation of TUPS-cystamine from unbound cystamine using a Sephadex G-25 gel filtration column, the yeast iso-1-cytochrome *c* was reduced and incubated with TUPS-cystamine in 150 mM HEPES (pH 8.5) and 0.2 M KCl for 4 h at 25 °C, and subsequently passed through a Sephadex G-25 column to remove salts and unbound TUPS-cystamine. The fractions that eluted in the void volume were collected and loaded onto a CM-Sephadex column to separate the unlabeled cytochrome *c* from TUPS-labeled cytochrome *c*. The TUPS−cytochrome *c* fraction was eluted by a linear 0 to 0.5 M KCl gradient and appeared at 100−150 mM KCl. Titration of this fraction with 5,5′-dithiobis(2-nitrobenzoic acid) indicated no free SH groups in the protein, confirming that the dye is linked to cytochrome *c* via its cysteine residues (*16*). The unlabeled cytochrome *c* eluted at 300 mM KCl. The TUPS−cytochrome *c* complex was concentrated by lyophilization, and the lyophilized sample was dissolved in a small volume of water, passed through a Sephadex G-25 column, and stored at −20 °C. HPLC analysis showed a single elution peak when monitored at either 550 or 373 nm. Spectra of this fraction confirmed the presence of the TUPS−cytochrome *c* complex. No other species eluted at other times when analyzed at various wavelengths, and we concluded that the TUPS−cytochrome *c* preparation is pure, with no free TUPS present. The same results were obtained for a fresh sample and a sample that had been incubated for 30 h at 25 °C.

The cytochrome *c* oxidase concentration, which equals half the heme A concentration, was determined spectrophotometrically using extinction coefficients of 159.2 mM^{-1} cm^{-1} at 420 nm and 17 mM^{-1} cm^{-1} at 598 nm for the fully oxidized enzyme and 212.8 mM^{-1} cm^{-1} at 444 nm and 39.8 mM^{-1} cm^{-1} at 604 nm for the reduced enzyme (*3*, *15*).

Intramolecular electron transfer in the TUPS−cytochrome *c*/cytochrome *c* oxidase complex was investigated following laser excitation of TUPS by a Nd:YAG laser (355 nm, 7 ns duration). Ten milliliters of an equimolar mixture of TUPS−cytochrome *c* complex and cytochrome *c* oxidase in 10 mM HEPES (pH 7.5) or 10 mM MES (pH 6.0) was deoxygenated with Ar for ∼15 min, followed by the addition of glucose oxidase, catalase, and glucose (final concentrations of 250 μg/mL, 10 μg/mL, and 20 mM, respectively) to remove any residual oxygen. Time-resolved difference spectra (post-minus prephotolysis) were collected in both the visible and Soret regions at 20 time points between 100 ns and 200 ms after photolysis of the TUPS−cytochrome *c*/cytochrome *c* oxidase complex. Between recording of individual spectra at a certain time delay, the solution in a 20 mL Erlenmeyer flask was circulated into the cuvette (10 mm × 2 mm × 4 mm, lwh) using a peristaltic pump. The spectral changes were probed along the 10 mm path 90° to the laser photolyzing beam. The laser power was limited to 6 mJ/pulse to minimize

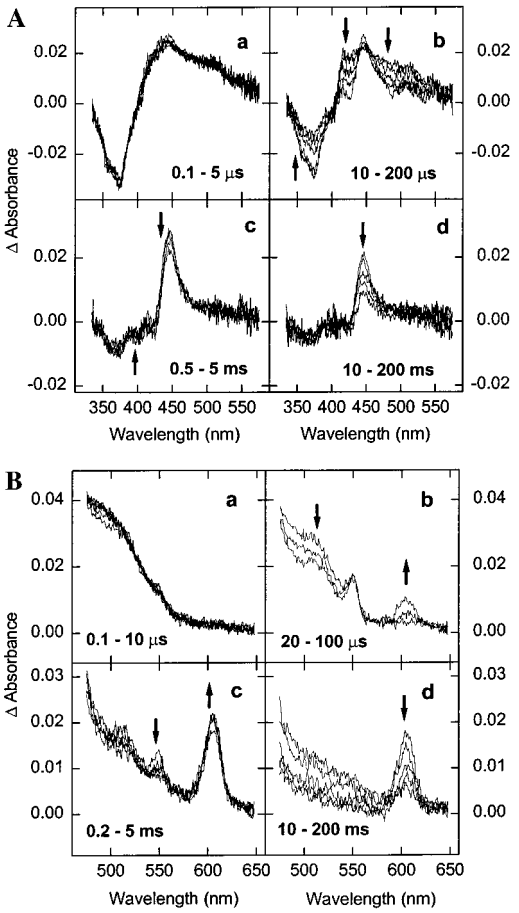

FIGURE 1: Time-resolved difference spectra (post- minus prephotolysis) in the Soret (A) and visible regions (B) collected during intramolecular electron transfer in the TUPS−cytochrome *c*/cytochrome *c* oxidase complex. The spectra represent 20 delay times following photoexcitation of TUPS. Three time points, spaced logarithmically, were recorded per decade. Each spectrum is an average of 16−32 accumulations. The arrows indicate the direction of the spectral changes with time. The TUPS−cytochrome *c*/cytochrome *c* oxidase complex concentrations were 7 and 20 μM in the Soret and visible regions, respectively. The buffer was 10 mM HEPES (pH 7.5), and the temperature was 25 °C.

direct photoreduction of the oxidase by the 355 nm laser pulse. The probe source was a pulsed xenon flash lamp, and appropriate filters restricted the probe beam to the spectral region of interest. Each spectrum (one time point) was an average of 16−32 single spectra. Three time points, spaced logarithmically, were recorded per decade. The measurements were carried out at 25 °C.

The time-resolved difference spectra were analyzed at all wavelengths and times simultaneously by SVD and global exponential fitting as previously described (*17*−*19*). The reduced **V** matrix was fitted with a sum of exponentials, which yielded the apparent (observed) rate constants and the corresponding spectral changes (*b*-spectra).

RESULTS

Spectral Changes during Intramolecular Electron Transfer. Figure 1 shows the time-resolved difference spectra (post- minus prephotolysis) in the Soret and visible regions after photoexcitation of the TUPS−cytochrome *c*/cytochrome *c* oxidase with a 355 nm laser pulse. The difference spectra can be interpreted in terms of absorbance changes of the

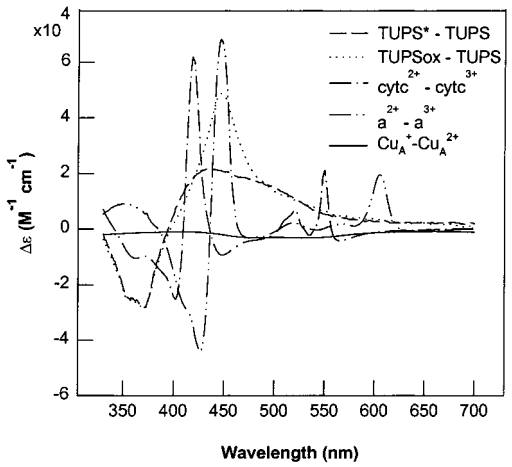

FIGURE 2: Transient difference spectra of the triplet TUPS minus the ground-state TUPS, the transient oxidized TUPS minus the ground-state TUPS, and the ground-state reduced-minus-oxidized difference spectra of heme *a*, cytochrome *c*, and Cu_A. The difference spectrum of Cu_A is from *T. thermophilus* (*20*). The difference spectrum of heme *a*, *without* the interference from Cu_A, was obtained by subtracting the spectrum of the mixed-valence CO complex and the reduced-minus-oxidized spectrum of Cu_A from the spectrum of the fully reduced CO-inhibited enzyme.

dye, the hemes of cytochrome *c* and cytochrome *c* oxidase, and Cu_A of cytochrome *c* oxidase. Figure 2 shows five difference spectra: the transient triplet TUPS (TUPS*) and the transient oxidized TUPS ($TUPS_{ox}$) versus the ground state spectrum of the TUPS and the steady-state reduced-minus-oxidized difference spectra of cytochrome *c*, heme *a*, and Cu_A. The difference spectrum of Cu_A is from *Thermus thermophilus* (*20*). The difference spectrum of heme *a*, without interference from Cu_A, was obtained by subtracting the spectrum of the mixed-valence CO complex and the reduced-minus-oxidized spectrum of Cu_A from the spectrum of the fully reduced CO-inhibited enzyme. The difference spectra of TUPS* and $TUPS_{ox}$ both have a trough of the same amplitude at ~370 nm, which is due to the photolyzed TUPS, while $TUPS_{ox}$ has a significantly larger absorbance at ~445 nm.

Qualitatively, the time-resolved difference spectra indicate that cytochrome *c* becomes reduced in the first 50 μs as shown by an absorbance increase at 550 nm (Figure 1B, panel b). Subsequent oxidation of cytochrome *c* occurs on the same apparent time scale as the reduction of heme *a* (Figure 1B, panel c). On a millisecond time scale, heme *a* is reoxidized, which is reflected by a decrease in absorbance at 605 nm. A comparison of Figures 1 and 2 shows that the triplet state is formed faster than 100 ns after photolysis, prior to any intramolecular electron transfer (Figure 1, panels a). This is in agreement with previous findings (*13*). A small increase in absorbance at 605 nm resulting from direct reduction of the cytochrome *c* oxidase by the laser pulse was subtracted from the data.

We also attempted to determine the contribution of Cu_A to the overall absorbance changes by monitoring the kinetics at 830 nm, where the contribution of the Cu_A is maximal and the contribution from the hemes is minimal. However, the significant absorbance of the dye at this wavelength, combined with the low extinction coefficient of Cu_A at 830 nm, made it impossible to extract meaningful spectral information at this wavelength.

*Different Fates of TUPS**. It is safe to assume that the reduction of cytochrome *c* results from electron transfer from the excited triplet of the dye. In the experiments reported here, laser photolysis converted ~13−15% of TUPS to the triplet state at a laser power of 6 mJ/pulse. Higher-energy laser pulses resulted in significant direct photoreduction of the cytochrome *c* oxidase. A fraction of TUPS* returned to the ground state on a microsecond time scale, presumably through quenching. This is reflected by the partial disappearance of the negative trough at ~370 nm (Figure 1A, panel b), which indicates the recovery of the reduced dye from its triplet state parallel with the reduction of cytochrome *c*.

In addition, our mechanistic analysis indicated an additional fraction of TUPS* not involved in electron transfer to cytochrome *c*. This fraction is not due to a contaminant, since HPLC and spectral analysis shows that the TUPS−cytochrome *c* complex is pure and contains no spectrally detectable contaminants, such as free TUPS. The fraction of TUPS* not involved in electron transfer to cytochrome *c* was also observed in experiments with the TUPS−cytochrome *c* complex in the absence of cytochrome *c* oxidase, and it decayed on a time scale similar to that observed in the presence of cytochrome *c* oxidase (not shown). Therefore, it does not appear that the interaction between the TUPS−cytochrome *c* complex and cytochrome *c* oxidase is perturbing the TUPS−cytochrome *c* complex. We have also shown that the apparent rate of cytochrome *c* reduction and the apparent rate of cytochrome *c* reoxidation and heme *a* reduction are independent of the concentrations of cytochrome *c* and cytochrome *c* oxidase (*16*). This is consistent with an intramolecular, and not a bimolecular, reaction between TUPS* and cytochrome *c* or cytochrome *c* oxidase, providing further evidence that free TUPS is absent.

It is possible that a fraction of the TUPS binds nonspecifically to the cytochrome *c* and that this complex is not electron transfer active. Repeated experiments have shown that this fraction does not interfere with analysis of the electron transfer from TUPS* to cytochrome *c*, because the decay of this fraction involves a separate parallel pathway. Thus in essence, the data can be analyzed by two *parallel* sequential pathways, one involving electron transfer from TUPS* to cytochrome *c* and subsequently to cytochrome *c* oxidase and a second one involving TUPS* not participating in electron transfer to cytochrome *c*. In the kinetic analysis discussed below, the spectral contribution due to TUPS* not involved in electron transfer to cytochrome *c* has been subtracted from the experimental data.

The time-resolved difference spectra were analyzed by SVD and global exponential fitting in both the visible and Soret regions. We have previously used this approach to extract spectra of intermediates involved in the reduction of dioxygen to water, and these spectra were in excellent agreement with model spectra of the proposed intermediates (*19*). The data reported here can be fitted with three exponentials, with apparent lifetimes of 23 ± 5 μs, 116 ± 15 μs, and 24 ± 8 ms in the Soret region and 30 ± 5 μs, 115 ± 15 μs, and 32 ± 8 ms in the visible region. The correction procedure discussed above had no effect on the apparent lifetimes. The spectral changes associated with the apparent lifetimes (*b*-spectra) and the residuals from the three-exponential fit are shown in Figure 3 for the Soret and visible regions.

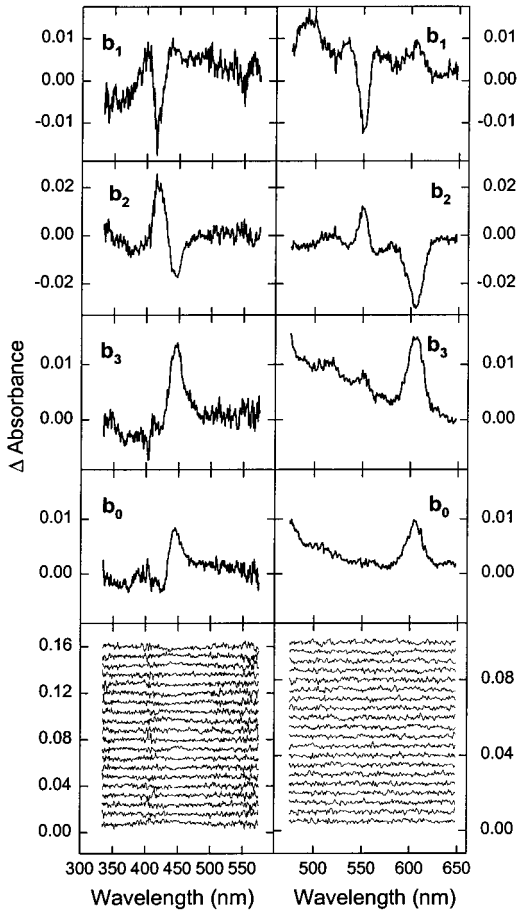

FIGURE 3: Spectral changes (*b*-spectra) from a three-exponential fit of the time-resolved Soret and visible data (referenced vs the ground state) and the residuals. The apparent lifetimes were 23 μs for b_1, 116 μs for b_2, and 24 ms for b_3 in the Soret region. In the visible region, the apparent lifetimes were 30 μs for b_1, 115 μs for b_2, and 32 ms for b_3. The residuals represent the absorbance difference of the data and the least-squares fit at each delay time. The delay times decrease from top to bottom. The residuals are separated by a constant value for clarity.

Qualitative information can be gained from the *b*-spectra. The first *b*-spectrum (b_1) with a trough at 550 nm reflects the reduction of cytochrome *c*, while the second *b*-spectrum (b_2) with a peak at 550 nm and a large trough at 604 nm represents the oxidation of cytochrome *c* and reduction of heme *a*. The peak at ~604 nm in the third *b*-spectrum (b_3) reflects the oxidation of heme *a* and return to the ground state. The non-zero time-independent spectrum b_o, which represents the spectrum extrapolated to infinite time, and the deviations in the residuals on the late millisecond time scale indicate that a small fraction of heme *a* becomes reoxidized on a longer time scale. The possible source of this reduced heme *a* could be a small amount of reducing agent, which would reduce the oxidized TUPS, thus maintaining heme *a* in its reduced state, analogous to what is observed in the Ru experiments using sacrificial electron donors (*7*, *9*).

When the data were fitted with four apparent lifetimes, with an additional apparent lifetime of 180 ± 40 ms, the residuals in the late millisecond region improved and spectrum b_o exhibited no spectral features. However, the spectral changes (*b*-spectra) associated with the two millisecond processes, although significantly different in amplitude, had similar shapes that are characteristic of the reduced-minus-oxidized difference spectrum of heme *a*.

Scheme 1: Proposed Mechanism for Intramolecular Electron Transfer in the Cytochrome *c*/Cytochrome *c* Oxidase Complex[a]

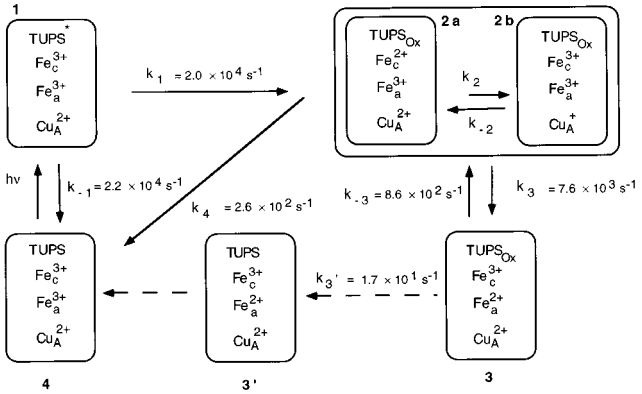

[a] The dashed arrows account for the slowly recovering portion of reduced heme *a*.

Moreover, since the data collection ends at 200 ms, the longest lifetime is highly uncertain and the underlying physical process is obscure. In view of this, our kinetic analysis was based on the three-exponential fit.

The SVD and global exponential fitting provide information about the minimum number of processes that are present, the apparent lifetimes, and the respective *b*-spectra (*17*−*19*). The *b*-spectra do not represent the true difference spectra of the intermediates present unless the pathway is unidirectional and the apparent lifetimes are at least an order of magnitude apart. In general, the *b*-spectra are linear combinations of intermediates, which is a complex function of the mechanism of the reaction. For a unidirectional pathway, the apparent lifetimes would equal the microscopic rate constants.

Kinetic Mechanism and Spectra of Intermediates. A reaction mechanism responsible for the observed spectral changes and the apparent lifetimes should start with a branching step to account for both the electron transfer from the triplet to cytochrome *c* and the quenching of the triplet. It also needs to represent subsequent electron transfer to oxidized heme *a*, and back from reduced heme *a* to the oxidized dye. Scheme 1 shows a mechanism that meets these requirements. The resulting data set was fitted to this mechanism, and the microscopic rate constants were adjusted until (a) the calculated apparent lifetimes were equal to the experimental lifetimes and (b) the experimentally extracted difference spectra of the intermediates matched those of the proposed (model) difference spectra of the intermediates depicted in Scheme 1.

The experimental difference spectra and the respective model difference spectra of intermediates **1**, **2**, and **3** are shown in Figure 4. The model spectra are a linear combination of the difference spectra of heme *a*, cytochrome *c* and Cu_A, TUPS*, and $TUPS_{ox}$ shown in Figure 2. The excellent agreement between the experimental and model difference spectra strongly supports the proposed mechanism. The concentration−time profiles of all the intermediates are shown in Figure 5 for both the visible (dotted line) and Soret (solid line) regions.

DISCUSSION

The results reported here show that Cu_A is the initial acceptor of electrons from cytochrome *c*, in agreement with

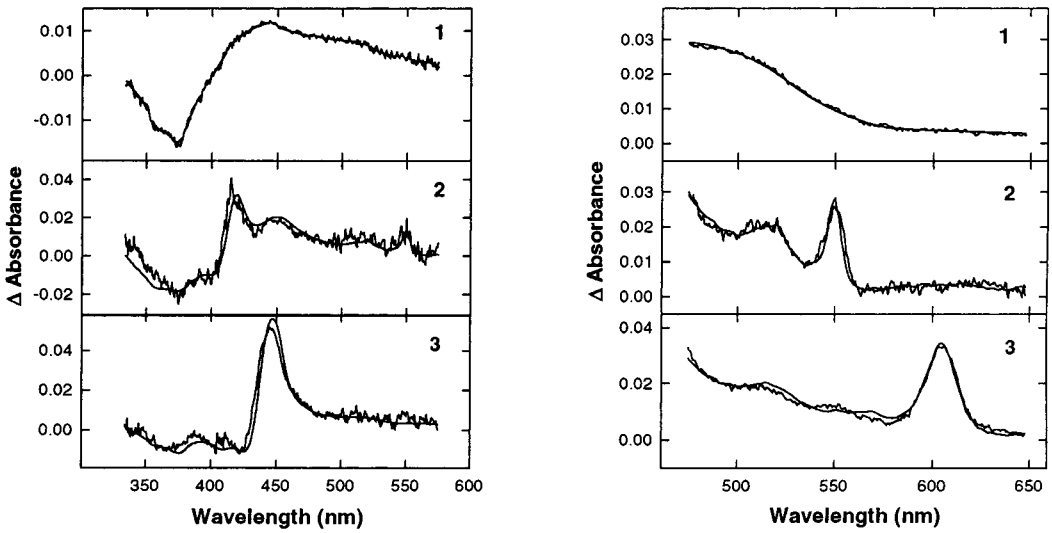

FIGURE 4: Comparison of the experimental and model difference spectra of intermediates **1**, **2**, and **3** in the proposed kinetic scheme (Scheme 1). The spectra were referenced to the prephotolysis TUPS−cytochrome *c*/cytochrome *c* oxidase complex. Panels 1−3 represent the difference spectra of intermediates **1**, **2** (**2a** and **2b**), and **3**, respectively. The experimental difference spectra were determined on the basis of the mechanism and the microscopic rate constants in Scheme 1. The model spectra are a linear combination of the difference spectra of heme *a*, cytochrome *c* and Cu_A, TUPS*, and $TUPS_{ox}$ shown in Figure 2.

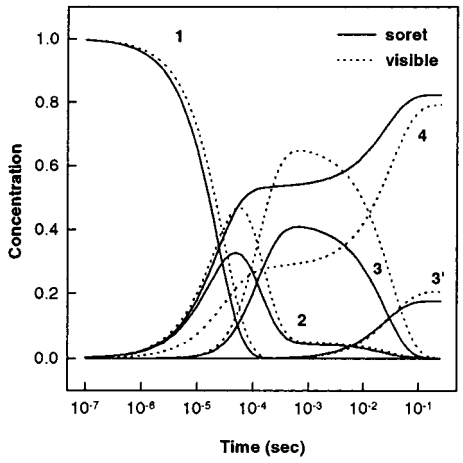

FIGURE 5: Time-dependent intermediate concentration profiles normalized to the photolyzed dye. The profiles are based on the mechanism and microscopic rat constants in Scheme 1.

previous studies on intramolecular electron transfer in the oxidized enzyme (*4*, *6*, *7*, *9*), the cytochrome *c*/cytochrome *c* oxidase complex using flow-flash (*12*), and the three-electron-reduced CO-inhibited enzyme using the perturbation method (*11*). As indicated in Scheme 1, the equilibrium between Cu_A and heme *a* is heavily shifted in the forward direction toward the reduction of heme *a*. This is in agreement with recent results on the oxidized enzyme using Ru-modified cytochrome *c* derivatives (*9*). The good agreement between the TUPS results and earlier reports confirms that TUPS is a useful method for initiating electron transfer in cytochrome *c* oxidase. Moreover, these studies and experiments carried out using single-wavelength detection (*16*) indicate that the maximum efficiency in terms of the reduced cytochrome *c* produced by a single laser pulse is significantly higher than that attained in previous studies using Ru−cytochrome *c* derivatives (*7*, *9*).

Electron Transfer between Cytochrome c and Cu_A. The use of three apparent lifetimes, including two on a microsecond time scale, does not allow us to resolve intermediates **2a** and **2b**, but the equilibrium constant can be determined. To obtain a good correspondence between the experimental and the model intermediate spectra, we need to include 60−80% of intermediate **2a** and 20−40% of intermediate **2b**. This indicates that the electron transfer between cytochrome *c* and Cu_A is back-shifted toward the reduced cytochrome *c* (intermediate **2a**).

It should be noted that the spectrum of Cu_A used in our analysis is from *T. thermophilus* (*20*). We have previously used the Cu_A spectrum from *Thermus* to extract the UV−visible spectra of intermediates present during the reduction of dioxygen to water (*19*). In these experiments, there was a good correspondence between the experimental and model spectra in the Cu_A spectral region (480−550 nm). When the Cu_A spectrum was omitted from the analysis, a significant deviation between the experimental and model spectra in the 480−550 nm region was observed (*18*). Thus, the Cu_A spectrum from *T. thermophilus* appears to be a useful model for that of bovine Cu_A. However, because the Cu_A absorbance is relatively small in the 480−550 nm region (Figure 2), our model in Scheme 1 would not be sensitive to small variations between the bovine and *T. thermophilus* spectra. It should be emphasized that the conclusion that the electron transfer from cytochrome *c* to heme *a* involves Cu_A is not based on the contribution of Cu_A in the 480−550 nm region, but rather on the amplitudes of the reduced-minus-oxidized cytochrome *c* and heme *a* spectra necessary to fit the data in both the visible and Soret regions.

Single-wavelength measurements at 550 and 604 nm in our laboratory on the intramolecular electron transfer in the cytochrome *c*/cytochrome *c* oxidase complex using photoexcitation of TUPS did not provide direct evidence that Cu_A is the initial acceptor of electrons from cytochrome *c* because the amount of reduced Cu_A (intermediate **2b**) could not be easily deduced (*16*). In these experiments, the apparent rate constant for the oxidation of cytochrome *c* was found to equal that of heme *a* reduction. Although single-wavelength measurements provide accurate time dependence, their spectral information is limited and complex mechanisms such

as Scheme 1 are not readily derived. In the absence of a mechanism, the microscopic rate constants are often mistakenly identified with the observed apparent rates, which is perhaps the biggest drawback of single-wavelength measurements. The amplitudes of both the reduced cytochrome *c* and heme *a* spectra depend on the equilibrium constant and the apparent lifetimes. The Appendix shows this complex relationship for a three-intermediate branched scheme. Additional steps such as in Scheme 1 would further complicate the analysis.

We were unable to resolve the rate of electron transfer from cytochrome *c* to Cu_A using three exponentials, presumably because this step is faster than the electron transfer from TUPS* to the oxidized heme of cytochrome *c*, which has a forward rate constant of $2.0-2.5 \times 10^4$ s^{-1} (Scheme 1) (see below). In comparison, a rate constant for electron transfer from the excited-state Ru(II*) modified at residue 39 to the heme of cytochrome *c* was reported to be 6×10^5 s^{-1} (*9*). The relatively slow rate of electron transfer from TUPS* to the heme of cytochrome *c* compared to the Ru−cytochrome *c* system most likely reflects a more efficient electron transfer pathway from residue 39 to the heme of cytochrome *c* than from Cys102 (*21*, *22*). Labeling alternative residues (mutated to cysteine) closer to the putative cytochrome *c* binding site would allow us to increase the rate of electron transfer between TUPS and cytochrome *c* beyond the rate of electron transfer between cytochrome *c* and Cu_A, thus avoiding the rate limitation imposed by the electron transfer from TUPS* to cytochrome *c*. Different driving forces and reorganization energies for the TUPS- and Ru-photoinduced reactions might also contribute to a difference in the electron transfer rates.

The rate constants observed for the return of the triplet back to the ground state (k_{-1}) were 2.2×10^4 s^{-1} in the Soret region and 7.8×10^3 s^{-1} in the visible region. The difference in the two rate constants, which accounts for the difference in the first apparent lifetime (23 vs 30 μs), reflects the different amounts of triplet quenched in the two experiments. The different extent of quenching could also account for the difference between our first apparent lifetimes and that found in the single-wavelength experiments (13 μs) (*16*). The time dependence of the concentration of the reduced cytochrome *c* at 550 nm in the single-wavelength experiments provides only the apparent rate constant of the first "process" ($k_1 + k_{-1}$), and *not* the true electron transfer rate between the triplet and oxidized cytochrome *c* (Appendix).

We have attempted to estimate the lower limit of the apparent rate constant for electron transfer between cytochrome *c* and Cu_A by including an additional apparent lifetime on the microsecond time scale. To obtain good correspondence between experimental and model difference spectra, the lower limits of the microscopic rate constants for the forward (k_2) and reverse (k_{-2}) directions must be 7.5×10^4 and 1.1×10^5 s^{-1}, respectively, giving a lower limit of the apparent rate constant for this step of 1.9×10^5 s^{-1} ($k_2 + k_{-2}$). The forward rate constant of 7.5×10^4 s^{-1} is in good agreement with estimated values based on flow-flash studies of the electrostatic cytochrome *c*/cytochrome *c* oxidase complex (*12*) and that obtained using Ru-modified cytochrome *c* as the source of photoinduced electrons (*9*). It should be emphasized that extracting these two rate constants by incorporating an additional lifetime is possible because of the wide spectral range that was studied, and would not have been feasible using single-wavelength measurements. We have recently employed a similar approach to determine the lower limit of the true rate constant for the electron transfer between heme *a* and Cu_A, and the good agreement between our values and theoretical values supports the validity of this type of analysis (*23*).

Equilibrium Constant for the Electron Transfer between Cytochrome c and Cu_A. The equilibrium constant for the electron transfer between Cu_A and cytochrome *c* based on both the Soret and visible regions is 0.25−0.67. Despite the uncertainty in the equilibrium constant, it is clear that this reaction is favored in the backward direction, that is, toward the reduced cytochrome *c*. Previous studies using laser-induced electron injection from Ru-modified cytochrome *c* have suggested that the equilibrium is heavily shifted in the forward direction toward Cu_A reduction (*9*). In both our case and the Ru-modified cytochrome *c*, the redox potential of the modified cytochrome *c* was the same as for wild-type cytochrome *c* (250−260 mV).

The difference between the two experiments is that the Ru system used sacrificial electron donors, aniline and 3-carboxyl-2,2,5,5-tetramethyl-1-pyrolidinyloxy (3CP), while this was not the case in our studies. In the absence of a sacrificial donor, Ru(III), which is generated upon electron transfer from Ru(II*) to oxidized cytochrome *c*, reoxidizes the reduced cytochrome *c*, returning to the ground state with a rate constant of 1×10^6 s^{-1} [see Scheme 1 in Pan et al. (*7*) and Geren et al. (*9*)]. In the presence of cytochrome *c* oxidase, this reoxidation of cytochrome *c* by Ru(III) would significantly lower the yield of Cu_A and heme *a* being reduced by cytochrome *c*. To prevent the reoxidation of cytochrome *c* by Ru(III), aniline and 3CP were included (*9*). In our case, no sacrificial electron donors are needed because the rate constant for the reoxidation of the reduced cytochrome *c* by $TUPS_{ox}$ (k_4) is small. However, in our system we have oxidized TUPS present, which may affect the reduction potentials of cytochrome *c* or Cu_A, and thereby shift the equilibrium toward the reduced cytochrome *c*.

Electron Transfer between Cu_A and Heme a. The electron transfer from Cu_A to heme *a* is heavily favored in the direction of the reduced heme *a*, with forward (k_3) and reverse (k_{-3}) rate constants of 7.6×10^3 and 8.6×10^2 s^{-1}, respectively, in agreement with previous studies (*7*, *9*). The rate constant k_3' represents the small fraction of heme *a* remaining in a reduced state on a long time scale.

In conclusion, these studies represent the first use of an optical multichannel analyzer in detecting time-resolved absorption changes during intramolecular electron transfer in the electrostatic cytochrome *c*/cytochrome *c* oxidase complex. We have shown that intramolecular electron transfer in the cytochrome *c*/cytochrome *c* oxidase complex can be investigated by photoexcitation of TUPS covalently bound to cysteine on cytochrome *c*. Our multichannel and single-wavelength measurements (*16*) have shown that the triplet state of TUPS is generated with high quantum efficiency. Using multichannel time-resolved optical spectroscopy, combined with SVD and global exponential fitting, we have extracted the spectra of the intermediates involved and the microscopic rate constants of all the steps. We have previously used the same analysis to extract the spectra of intermediates involved in the reduction

of dioxygen to water at different pHs (*19*, *23*).

Our data confirm previous results that Cu_A is the initial electron acceptor from cytochrome *c*. Furthermore, they show that the electron transfer between cytochrome *c* and Cu_A is rate-limited by electron transfer from TUPS* to cytochrome *c*, and that the equilibrium for electron transfer between cytochrome *c* carrying the oxidized TUPS and Cu_A is favored in the direction of reduced cytochrome *c* and oxidized Cu_A. Studies aimed at labeling alternative residues (mutated to cysteine) closer to the putative cytochrome *c* binding site to circumvent the rate limitation imposed by the electron transfer from TUPS* to cytochrome *c* are underway.

Our multichannel data also allow us to follow the spectral changes of the dye that occur during electron transfer to cytochrome *c*. This adds complexity to the data and the proposed model, but at the same time, it allows us to determine the true rate of cytochrome *c* reduction, providing additional support for the proposed mechanism. Moreover, we were able to detect the TUPS* not involved in electron transfer to cytochrome *c*, an observation only possible with the multichannel detection, SVD, and global exponential fitting approach. Single-wavelength experiments (*16*) failed to elucidate this fraction, because the experiments were carried out at wavelengths in which the contribution of the dye was small. However, our analysis shows that this fraction decays by a separate pathway and therefore can be subtracted from the spectra.

Our studies extend previous investigations of intramolecular electron transfer in the cytochrome *c*/cytochrome *c* oxidase complex using Ru−cytochrome *c* derivatives and single-wavelength detection (*7*, *9*). The multiwavelength detection, SVD, and global fitting approach provides information about electron transfer rates in the forward direction and allows us to extract information regarding back rates when the system relaxes to its initial state, which is generally ignored in single-wavelength studies.

APPENDIX

Relationship between Kinetic Parameters and the Time Dependence of Intermediate Concentrations. Reduced cytochrome *c* has a characteristic absorption maximum at 550 nm, and this wavelength is often used to monitor the oxidation of cytochrome *c*. The time dependence of the concentration of the reduced form is typically obtained by subtracting absorption changes at a reference wavelength from the absorption changes recorded at 550 nm. Although the time-dependent concentration profiles of the single-wavelength experiments are generally very accurate, the exponential fits to these traces can be difficult to interpret. The direct assignment of true electron transfer rates to exponentials is an oversimplification of the kinetic problem and can lead to incorrect conclusions. The direct assignment is valid for only a limited number of kinetic schemes, such as a unidirectional sequential model, but is not valid for the branched mechanism shown in Scheme 1. To illustrate the complexity of the kinetic analysis, we show below the analytical solution to a simplified branched kinetic scheme.

The mechanism in Scheme 1 includes a branch (k_1 and k_{-1}), in addition to reversible steps, and therefore cannot be easily solved analytically. However, it can be approximated by the following simplified mechanism, which is easier to solve and is sufficient for our discussion:

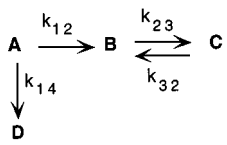

(1)

The time dependence of the intermediate concentrations is described by a set of linear first-order differential equations:

$$d\mathbf{c}/dt = \mathbf{M}\mathbf{c} \tag{2}$$

where **c** is the concentration vector and **M** is the kinetic matrix, constructed from the microscopic rates connecting the intermediates according to

$$\mathbf{M} = \begin{bmatrix} -(k_{12}+k_{14}) & 0 & 0 & 0 \\ k_{12} & -k_{23} & k_{32} & 0 \\ 0 & k_{23} & -k_{32} & 0 \\ k_{14} & 0 & 0 & 0 \end{bmatrix} \tag{3}$$

The solution to eq 1 can be written in terms of eigenvectors, $\mathbf{X}_i$, and eigenvalues (λ_i) of the kinetic matrix, **M**:

$$\mathbf{c} = \sum f_i \mathbf{X}_i \exp(\lambda_i t) \tag{4}$$

The constants f_i can be determined from the initial conditions. Both the eigenvalues and eigenvectors are obtained by solving the following equation

$$(\mathbf{M} - \lambda\mathbf{E})\mathbf{X} = 0 \tag{5}$$

where **E** is the identity matrix.

The apparent rate constants α are the eigenvalues of the kinetic matrix with the sign reversed, and the eigenvectors represent the composition of the so-called *b*-spectra. The apparent rates for the kinetic mechanism in eq 1 are as follows:

$$\alpha_1 = (k_{12}+k_{14}) \quad \text{spectrum } b_1\ (X_1)$$

$$\alpha_2 = (k_{23}+k_{32}) \quad \text{spectrum } b_2\ (X_2)$$

$$\alpha_3 = 0 \quad \text{spectrum } b_3\ (X_3)$$

The compositions of the *b*-spectra are given by the scaled eigenvectors. The scaling is done by matching the initial conditions; that is, the sum of the eigenvectors should produce the concentration vector at time zero.

$$\sum f_i \mathbf{X}_i = X_{\text{time}=0} = \begin{pmatrix} c_0 \\ 0 \\ 0 \\ 0 \end{pmatrix} \tag{6}$$

The expressions for the eigenvectors can be simplified by introducing the equilibrium constant, *K*, and the branching ratio, *R*:

$$K = \frac{k_{23}}{k_{32}} \quad R = \frac{k_{12}}{(k_{12}+k_{14})}$$

The eigenvectors arranged in a matrix are shown below. Each column represents an eigenvector, or *b*-spectrum, corresponding to an apparent rate, with four components that are the contributions of intermediates **A**, **B**, **C**, and **D** to the *b*-spectrum.

$$\begin{bmatrix} x_{11} = c_0 & x_{12} = 0 & x_{13} = 0 \\ x_{21} = -\dfrac{(1+K)\alpha_1 - \alpha_2}{(1+K)(\alpha_1 - \alpha_2)}Rc_0 & x_{22} = \dfrac{K\alpha_1}{(1+K)(\alpha_1 - \alpha_2)}Rc_0 & x_{23} = \dfrac{1}{1+K}Rc_0 \\ x_{31} = \dfrac{K\alpha_2}{(1+K)(\alpha_1 - \alpha_2)}Rc_0 & x_{32} = -\dfrac{K\alpha_1}{(1+K)(\alpha_1 - \alpha_2)}Rc_0 & x_{33} = \dfrac{K}{1+K}Rc_0 \\ x_{41} = -(1-R)c_0 & x_{42} = 0 & x_{43} = (1-R)c_0 \end{bmatrix}$$

Each row in the eigenvector matrix corresponds to an intermediate, and contains the amplitudes of the exponential forms that describe the time dependence of the intermediate concentration.

$$\begin{aligned} c_{\mathbf{A}} &= c_0 e^{-\alpha_1 t} \\ c_{\mathbf{B}} &= x_{21} e^{-\alpha_1 t} + x_{22} e^{-\alpha_2 t} + x_{23} \\ c_{\mathbf{C}} &= x_{31} e^{-\alpha_1 t} + x_{32} e^{-\alpha_2 t} + x_{33} \\ c_{\mathbf{D}} &= x_{41} e^{-\alpha_1 t} + x_{43} \end{aligned} \tag{7}$$

Intermediate **B** represents cytochrome *c* in Scheme 1. The single-wavelength recording at 550 nm should be described by the time-dependent concentration, $c_{\mathbf{B}}$, of this intermediate. It is clear that the rise of the cytochrome *c* signal is faster than the true electron transfer rate, which can only be obtained if the branching ratio is known from additional spectral information. Equation 7 shows that the time-dependent concentration, $c_{\mathbf{B}}$, is a complex function of the equilibrium constant, *K*, the branching ratio, *R*, and the apparent lifetimes, α_1 and α_2, and therefore is not easily deduced from single-wavelength measurements.

Because of the spectral overlap between TUPS, cytochrome *c*, and heme *a*, it is difficult to find spectral regions where individual intermediate forms can be recorded separately, which is the ultimate goal in single-wavelength experiments. This limitation can be overcome by multichannel wavelength recording and subsequent kinetic analysis using the SVD and global exponential fitting procedure.

REFERENCES

1. Cooper, C. E. (1990) *Biochim. Biophys. Acta 1017*, 187−203.
2. Wilson, M. T., Greenwood, C., Brunori, M., and Antonini, E. (1975) *Biochem. J. 147*, 145−153.
3. Antalis, T. M., and Palmer, G. (1982) *J. Biol. Chem. 257*, 6194−6206.
4. Kobayashi, K., Une, H., and Hayashi, K. (1989) *J. Biol. Chem. 264*, 7976−7980.
5. Farver, O., Einarsdóttir, Ó., and Pecht, I. (1999) *Eur. J. Biochem. 267*, 950−954.
6. Nilsson, T. (1992) *Proc. Natl. Acad. Sci. U.S.A. 89*, 6497−6501.
7. Pan, L. P., Hibdon, S., Liu, R.-Q., Durham, B., and Millet, F. (1993) *Biochemistry 32*, 8492−8498.
8. Brzezinski, P., Sundahl, M., Ädelroth, P., Wilson, M. T., El-Agez, B., Wittung, P., and Malmström, B. G. (1995) *Biophys. Chem. 54*, 191−197.
9. Geren, L. M., Beasley, J. R., Fine, B. R., Saunders, A. J., Hibdon, S., Pielak, G. J., Durham, B., and Millet, F. (1995) *J. Biol. Chem. 270*, 2466−2472.
10. Brzezinski, P., and Wilson, M. T. (1997) *Proc. Natl. Acad. Sci. U.S.A. 94*, 6176−6179.
11. Morgan, J. E., Li, P. M., Jang, D.-J., El-Sayed, M. A., and Chan, S. I. (1989) *Biochemistry 28*, 6975−6983.
12. Hill, B. C. (1991) *J. Biol. Chem. 266*, 2219−2226.
13. Kotlyar, A. B., Borovok, N., and Hazani, M. (1997) *Biochemistry 36*, 15823−15827.
14. Kotlyar, A. B., Borovok, N., and Hazani, M. (1997) *Biochemistry 36*, 15828−15833.
15. Yoshikawa, S., Choc, M. G., O'Toole, M. C., and Caughey, W. S. (1977) *J. Biol. Chem. 252*, 5498−5508.
16. Kotlyar, A. B., Hazani, M., Borovok, N., Szundi, I., and Einarsdóttir, Ó. (2000) *Eur. J. Biochem. 267*, 5805−5809.
17. Georgiadis, K. E., Jhon, N.-I., and Einarsdóttir, Ó. (1994) *Biochemistry 33*, 9245−9256.
18. Sucheta, A., Georgiadis, K. E., and Einarsdóttir, Ó. (1997) *Biochemistry 36*, 554−565.
19. Sucheta, A., Szundi, I., and Einarsdóttir, Ó. (1998) *Biochemistry 37*, 17905−17914.
20. Slutter, C. E., Sanders, D., Wittung, P., Malmström, B. G., Aasa, R., Richards, J. H., Gray, H. B., and Fee, J. A. (1996) *Biochemistry 35*, 3387−3395.
21. Wuttke, D. S., Bjerrum, M., Winkler, J. R., and Gray, H. B. (1992) *Science 256*, 1007−1009.
22. Beratan, D. N., Onuchic, J. N., Winkler, J. R., and Gray, H. B. (1992) *Science 258*, 1740−1741.
23. Paula, S., Sucheta, A., Szundi, I., and Einarsdóttir, Ó. (1999) *Biochemistry 38*, 3025−3033.

BI002341V